Cancer Research

Hypoxia Predicts Aggressive Growth and Spontaneous Metastasis Formation from Orthotopically Grown Primary Xenografts of Human Pancreatic Cancer

Qing Chang[1], Igor Jurisica[1,2], Trevor Do[1], and David W. Hedley[1,2,3]

Abstract

Hypoxia in solid tumors is associated with treatment resistance and increased metastatic potential. Although hypoxia has been reported in pancreatic cancer patients, there is little direct evidence that this contributes to their overall poor prognosis. To address this, we examined the associations between hypoxia and biological aggression in a series of patient-derived xenografts grown orthotopically. Early passage xenografts were established from 16 patients undergoing surgery for pancreatic cancer and maintained in the pancreas of immune-deprived mice. Hypoxic cells were labeled using the 2-nitroimidazole probe EF5 and stained for immunofluorescence microscopy of tissue sections or as cell suspensions for flow cytometry. Bromodeoxyuridine (BrdUrd) uptake, microvessel density, cleaved caspase-3, and the differentiation markers E-cadherin, cytokeratin 19, and vimentin were analyzed in relation to hypoxia. Orthotopic implants closely resembled the histology of the original surgical samples. The 16 primary xenografts showed a wide range in their growth rates and metastatic potential, reminiscent of the spectrum of behavior seen in the clinic. EF5 labeling, tumor growth rates, and metastatic patterns were highly consistent within replicates, indicating a significant transmissible (genetic or epigenetic) component. Hypoxia was highly correlated with rapid tumor growth, increased BrdUrd uptake, and with spontaneous metastasis formation. mRNA expression analysis showed increased expression of genes involved in cell survival and proliferation in the hypoxic models. The results suggest that hypoxia is a major adverse prognostic factor in pancreatic cancer patients and support the introduction of techniques to measure hypoxia directly in patients and the development of treatment protocols to target hypoxia. *Cancer Res; 71(8); 3110–20. ©2011 AACR.*

Introduction

Hypoxia occurs in solid tumors when the consumption of oxygen exceeds its delivery by the vascular system (1). In most large clinical studies, the outcome is worse for patients with hypoxic tumors, consistent with the long-held idea that hypoxia confers both radiation and chemotherapy resistance (2–4). Unexpectedly, high levels of tumor hypoxia were also found to predict metastasis development in patients treated by surgery alone, pointing to biological effects beyond those linked to drug and radiation resistance (5, 6).

The hypoxic microenvironment is hostile to cancer cell survival. Hypoxia tolerance can occur due to genetic changes such as p53 loss that enhance cell survival (7), or due to cellular responses to hypoxia, driven, for example, by hypoxia-inducible factors (HIF) or the unfolded protein response, that modify gene expression, cell phenotype, and metabolism (8, 9). In a recent article describing the genetic evolution of pancreatic cancers, it was suggested that cancer cells adapted to hypoxia could undergo additional genetic changes that enhance metastasis formation (10). In other words, hypoxia might be a cause of genetic change, as well as a consequence.

The increased metastatic potential of hypoxic cancers might result from changes in cell biology that are mediated by cellular responses to hypoxia (11–13). For example, growth under hypoxic conditions may reprogram epithelial cells toward a more mesenchymal phenotype due to the activation of E-cadherin transcriptional repressors (12, 14, 15). Cells undergoing epithelial-to-mesenchymal transition (EMT) show reduced cell–cell interaction via adherens junctions and increased extracellular matrix interactions via integrins/focal adhesion kinase. Consequently, they are more motile and can invade and metastasize (16, 17). Successful development of a metastasis presumably requires at least 1 cancer-initiating cell. Pancreatic cancer stem cells have been reported to show EMT features (18, 19), and it has also been proposed that

Authors' Affiliations: [1]Ontario Cancer Institute/Princess Margaret Hospital and the Campbell Family Institute for Cancer Research; [2]Department of Computer Science and Department of Medical Biophysics, University of Toronto; and [3]Department of Medical Oncology and Hematology, Princess Margaret Hospital, Toronto, Ontario, Canada

Note: Supplementary data for this article are available at Cancer Research Online (http://cancerres.aacrjournals.org/).

Corresponding Author: David W. Hedley, Department of Medical Oncology and Hematology, Princess Margaret Hospital, 610 University Avenue, Toronto, Ontario, Canada M5G 2M9. Phone: 416-946-2262; Fax: 416-946-6546; E-mail: david.hedley@uhn.on.ca

doi: 10.1158/0008-5472.CAN-10-4049

hypoxia provides a niche that favors the survival of cancer cells with stem-like properties (20–22).

Although pancreatic cancers are often considered as being hypoxic, most publications have used histologic surrogate markers for hypoxia that might be compromised by surgical ischemic time or by sampling error due to the heterogeneous distribution of hypoxia in tumor tissue (23, 24). Direct evidence that pancreatic cancers are hypoxic is limited to a small study in which intraoperative pO_2 measurements were made by inserting needle electrodes into the exposed tumor (25). To address the question of whether hypoxia plays an important role in pancreatic cancer patients, we studied a series of early passage xenografts established from pancreatectomy samples and grown orthotopically. The results show striking associations between hypoxia and aggressive growth and metastasis formation.

Materials and Methods

Establishment of orthotopic primary pancreatic cancer xenografts

Animal experiments were carried out using protocols approved by University Health Network Animal Welfare Committee. The primary pancreatic cancer xenografts were established as previously described (26–29). Fresh pancreatectomy samples that were superfluous to diagnostic needs were obtained from the University Health Network Tumor Tissue Bank according to institutional human ethical guidelines. Primary xenografts were established at the orthotopic site of 4- to 5-week-old severe combined immunodeficiency mice by attaching tumor fragments to the surface of the exposed pancreas by a small incision in the upper left abdomen under general anesthesia. Sixteen orthotopic primary pancreatic cancer xenografts, designated as Ontario Cancer Institute Pancreas (OCIP) 16, 18, 19, 20, 21, 23, 24, 28, 30, 34, 36, 37, 38, 40, 51, and 52, were used in this study. A minimum of 6 replicate tumors were used for each model.

Detection of tumor hypoxia and proliferation

To allow assessment of the hypoxic regions within tumors, mice were injected intravenously and intraperitonealy (i.p.) with the 2-nitroimidazole hypoxia marker agent EF5 (30 mg/kg) 4 hours prior to sacrifice, as described previously (30, 31). They were then injected i.p. with 100 mg/kg 5-bromo-2′-deoxyuridine (BrdUrd; Sigma) dissolved in PBS 30 minutes prior to sacrifice. Tumors without EF5 and BrdUrd injection were used as negative controls for each model. Tumors were then rapidly excised and bisected. One half was fixed and processed for paraffin embedding, and the other half disaggregated to a single-cell suspension for flow cytometric analysis.

Flow cytometric analysis

Single-cell suspensions from tumors were prepared by an enzymatic technique (Collagenase XI, Protease, and DNase I cocktail) for flow cytometry as described previously (32, 33). Aliquots of single-cell suspensions were then fixed either in 80% ethanol to allow DNA denaturation for anti-BrdUrd labeling or in 4% formaldehyde for 10 minutes to optimize intracellular protein staining. For dual EF5 and BrdUrd labeling, cells were acid denatured, neutralized, and then stained with anti-EF5 monoclonal antibody (Cy5 conjugates, ELK3-51, obtained from Dr. Cameron Koch, University of Pennsylvania), anti-BrdUrd (PRBQD-Alexa 488; Phoenix Flow Systems), and 1 μg/mL 4′,6-diamidino-2-phenylindole (DAPI). Anti-vimentin and anti-cytokeratin 19 (both from Abcam) were also used for staining. Samples were analyzed using an LSRII flow cytometer (BD Biosciences). Single-parameter DNA content histograms were analyzed using ModFit LT 3.0 (Verity). The percentages of EF5- and BrdUrd-positive cells were analyzed using WinList 6.0 (Verity).

Immunohistochemical and immunofluorescent staining

Serial sections were cut from paraffin-embedded tumor tissue, and stained with hematoxylin and eosin (H&E), Masson's trichrome, and for α-smooth muscle actin by immunohistochemistry (IHC; Dako A/S). The remaining sections were labeled for fluorescence microscopy, using primary antibodies against BrdUrd (Caltag), CD31 (Santa Cruz Biotechnology), cleaved caspase-3 (Cell Signaling Technology), E-cadherin (Vector Laboratories), and vimentin (American Research Products), respectively, and then dual labeled with an anti-EF5–Cy3 conjugate. Secondary Cy5-conjugated anti-mouse or anti-rabbit antibodies were used for indirect immunofluorescence staining (Jackson Laboratories). Secondary antibodies were used alone to control for nonspecific background. Sections were counterstained with 1 μg/mL DAPI to outline the nuclear area.

Image capture

Entire immunofluorescence-stained sections were imaged at 1-μm resolution, using a laser scanning system (TISSUEscope; Biomedical Photometrics), and composite images of regions of interest were imaged at higher resolution (magnification × 20), using a conventional fluorescence microscope and scanning stage (BX50; Olympus Corporation). Uncompressed TIFF images (8-bit) were acquired for analysis.

Image analysis

H&E images were reviewed to generate masks of viable tumor areas for individual images of immunofluorescence using image analysis tools developed in-house on the basis of IDL 6.3 programming language. Fluorescence of debris and other artifacts was omitted. Measurements of fluorescence intensity in viable tumor areas were done using Image-Pro Plus 6.1.0 (Media Cybernetics). Immunofluorescence intensity was visually inspected and EF5-positive labeling was represented by intensities above the 75th percentile [the 3rd quartile, (Q3)], as described previously (34). The integrated optical density and fractional labeled area were measured in viable tumor areas by using the Q3 threshold. The product of integrated optical density and fractional labeled area was calculated to represent relative protein abundance. Ratios of protein abundance in EF5-positive region and non-EF5 region of individual tumors were used to determine group

medians. The percentages of positive stained nuclei were measured for BrdUrd and cleaved caspase-3 analyses on the basis of binary images. Researchers were blinded to sample identity during analysis.

Reverse transcription and quantitative PCR

Total RNA was isolated from 3 frozen tumors of each model by homogenization in TRIzol reagent and acid phenol–chloroform extraction, purified by RNeasy mini kit (Qiagen). Reverse transcription was completed at 42°C with SuperScript II RNase H^- reverse transcription kit (Invitrogen). Quantitative PCR (qPCR) was conducted with 10 ng of the first-strand cDNA synthesis mixture as a template and individual primer sets (see Supplementary Information), using the SYBR Green PCR Master Mix and an Applied Biosystems 7900 HT instrument. Primers were designed using Primer Express 3.0 (Applied Biosystems). Gene expression levels in the samples were calculated relative to control, using the comparative C_t method (35): $\Delta\Delta C_t = \Delta C_{t\_sample} - \Delta C_{t\_control}$, fold change $= 2^{-\Delta\Delta Ct}$. The geometric mean of GAPDH, β-actin, TATA binding protein, and β-2-microglobulin were used to normalize the expression data (ΔC_t).

Protein–protein interaction analysis

Individual genes were mapped to proteins by using Interologous Interaction Database (I2D) version 1.9 (36). Only direct interactions of target proteins and direct interactions among their interactors were considered. The protein–protein interaction network was visualized and annotated in NAViGaTOR version 2.2.1 (37).

Statistical methods

The statistical significance of differences in numerical data was evaluated with a Student's t test, the statistical significance of correlation between different factors was evaluated with Pearson correlation analysis, and the statistical significance of comparison of survival curves was evaluated with the log-rank test. A P value of less than 0.05 was considered to be statistically significant. All statistical tests were 2-sided.

Results

Characterization of orthotopic primary pancreatic cancer xenografts

Clinicopathologic features and *K-ras* and *p53* mutation status of the 16 patient donors are shown in Table 1. Histologic examination of the H&E sections showed that the orthotopically grown primary xenografts were typically moderately well differentiated, mucin-secreting adenocarcinomas that closely resembled the original surgical specimen (Fig. 1). They were organized into glandular structures, with a prominent fibrovascular stroma replete with α-smooth muscle actin–positive mesenchymal stromal cells (Supplementary Fig. S1). Cellular DNA content analysis by flow

Table 1. Primary pancreatic cancer specimens

OCIP#	Diagnosis	Stage[a]	*K-ras* mutation[b]	p53 IHC[c]
16	Ductal ADC, MD	T3N1b	K12, GAT	−
18	Ductal ADC, MD	T3N0	K12, GAT	−
19	Ductal ADC, MD	T3N1b	K12, GAT	−
20	Ductal ADC, WD	T3N1b	K12, GTT	+
21	Ductal ADC, MD	T3N0	Wild-type	−
23	Ductal ADC, PD	T3N1b	K12, CGT	+
24	Ductal ADC, MD	T3N1a	K12, GAT	+
28	Ductal ADC, WD	T3N0	K12, GTT	−
30	Ductal ADC, MD	T3N1a	K12, CGT	−
34	Mucinous cyst ADC and invasive ADSQ	T3N1b	Wild-type	+
36	Ductal ADC, PD	T2N0	Wild-type	−
37	Ductal ADC, MD	T3N1b	K12, GAT	−
38	Ductal ADC, MD	T3N0	K12, GTT	−
40	Ductal ADC, MD	T3N1b	K12, GTT	−
51	Ductal ADC, MD	T4N0	K12, GAT	−
52	Ductal ADC, WD	T3N0M1	K12, GAT	−

Abbreviations: ADC, adenocarcinoma; ADSQ, adenosquamous carcinoma; WD, well-differentiated; MD, moderately differentiated; PD, poorly differentiated.

[a]TNM classification of tumors of the exocrine pancreas: T2, tumor limited to the pancreas, more than 2 cm in greatest dimension; T3, tumor extends directly into any of the following: duodenum, bile duct, peripancreatic tissues; T4, tumor extends directly into any of the following: stomach, spleen, colon, adjacent large vessels; N0, no regional lymph node metastasis; N1a, metastasis in a single regional lymph node; N1b, metastasis in multiple regional lymph nodes.

[b]Mutation occurs in "codon 12, base transition."

[c]Immunohistochemical staining for p53; "+", positive staining; "−", negative staining.

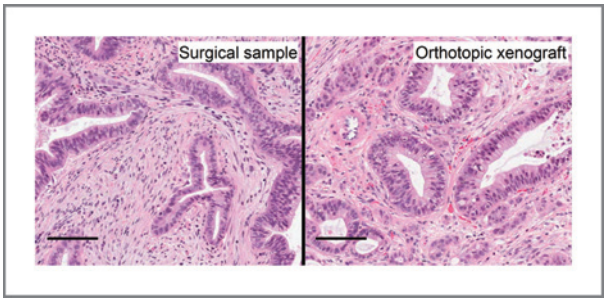

Figure 1. Orthotopic implants closely resemble the histology of the original surgical samples. Histologic sections of the original patient sample (left) and the orthotopically grown primary pancreatic cancer xenografts (right) stained with H&E. Scale bars, 100 μm.

cytometry confirmed that in many of these tumors, normal mouse cells accounted for more than 80% of the total cell population (Supplementary Fig. S2).

Growth rates correlate with BrdUrd uptake

Because the tumors were grown at the orthotopic site, their sizes were estimated by palpation and the passage time was used as a surrogate marker for the growth rate. Tumor growth rates were defined by the number of days between orthotopic implantation and growth to ~1-cm diameter. The primary xenografts showed a wide range in growth rates (i.e., passage times of 4–26 weeks), which correlated with BrdUrd incorporation assessed by immunofluorescent staining analysis (Pearson, $r = -0.7643$; $P = 0.0006$; Fig. 2A).

Tumor growth and metastasis rate

Mice were examined for the presence of metastases at the time of tumor resection, with histologic confirmation of suspicious lesions. As shown in Figure 2B, the gross metastasis patterns were similar to those seen in pancreatic cancer patients; by microscopy, they were also organized into glandular structures surrounded by stroma, similar to the appearance of the primary tumor. Spontaneous metastases to liver (OCIP23, 28, 36, 37, 38, 51, and 52) and lung (OCIP28) occurred. Malignant ascites also developed in 6 of the 10 fast growing models (OCIP21, 23, 28, 34, 36, and 52). The development of spontaneous metastases from the orthotopic site was highly correlated with the tumor growth rate ($P = 0.0002$) and BrdUrd incorporation ($P = 0.0003$), shown in Figure 2C.

Hypoxia measurements

Representative plots of EF5 labeling versus DNA content for the 16 primary xenografts are shown in Figure 3A. EF5 staining was low or absent in OCIP16, 18, 19, 24, 30, and 40 (top panel), whereas OCIP20, 21, 23, 28, 34, 36, 37, 38, 51, and 52 showed a heterogeneous distribution of positive staining similar to that previously reported (33, 38). Positive staining was seen both in the aneuploid cancer cells and in the normal mouse stroma. The percentages of EF5-positive cells were highly consistent within individual models. The tumors seemed to segregate into high and low EF5 labeling at a cutoff value of 5% positive EF5 labeling, with little overlap between the 2 groups ($P < 0.0001$; Fig. 3B).

Hypoxia and BrdUrd labeling

Dual immunofluorescence staining for EF5 and BrdUrd showed a striking loss of BrdUrd incorporation in the EF5-positive regions, indicating that hypoxia causes cell-cycle arrest in these models (Fig. 4A). Interestingly, hypoxia associated with cell-cycle arrest was also seen in small (<1 mm) liver metastases from the hypoxic models, suggesting that this might cause resistance to cell-cycle–active agents such as gemcitabine when used as adjuvant treatment (Fig. 4B). However, as shown in Figure 4C, overall the extent of BrdUrd labeling in the hypoxic models was significantly greater than that seen in the low EF5 staining tumors ($P = 0.0002$). This apparent paradox is accounted for by higher BrdUrd labeling in the better oxygenated regions of the hypoxic models, as seen in Figure 4A. Hypoxia was also associated with rapid growth ($P = 0.0002$) and with spontaneous metastasis formation ($P = 0.0003$).

Hypoxia and apoptosis

As shown in Supplementary Figure S3A, cleaved caspase-3 labeling of individual cells showed a heterogeneous distribution that seemed similar in the EF5-negative and -positive areas. However, regions surrounding necrotic areas were often densely populated by cleaved caspase-3–positive cells, as has been previously reported (7). When these regions were excluded, cleaved caspase-3 staining in viable tumor tissue of hypoxic models was significantly higher than in low EF5 staining models ($P = 0.0005$; Supplementary Fig. S3B).

Hypoxia and microvessel density

Consistently in these models, blood vessels were organized in the stroma surrounding the tumor nests and did not invade into masses of tumor tissue (Supplementary Fig. S4A), as has been observed by our group and others using cell line–derived xenografts (39, 40). Microvessel density and the percentage of CD31-positive pixel density obtained from the replicate tumors of 16 models are shown in Supplementary Figure S4B. No significant correlation between hypoxia and either marker of blood vessels was observed in these models.

Hypoxia and cell differentiation

Hypoxia has been reported to promote transition toward a more mesenchymal phenotype, associated with increased potential for metastasis (12, 15). We therefore searched for features of EMT in the hypoxic models. Representative dual immunofluorescence staining for EF5 and E-cadherin is shown in Supplementary Figure S5A. In all models tested, the cells within the hypoxic regions showed epithelial features similar to the nonhypoxic regions, including maintenance of apical/basal polarity, surface expression of E-cadherin, and negative staining for vimentin. Single-cell measurements by flow cytometry showed a striking heterogeneity in vimentin expression in the cancer cell population of some models, indicating a degree of plasticity toward expression of a mesenchymal marker (Supplementary Fig. S5B). However, vimentin expression was predominant in EF5-negative cells, indicating that it was not directly linked to hypoxia. Interestingly, vimentin-positive cells coexpressed the epithelial

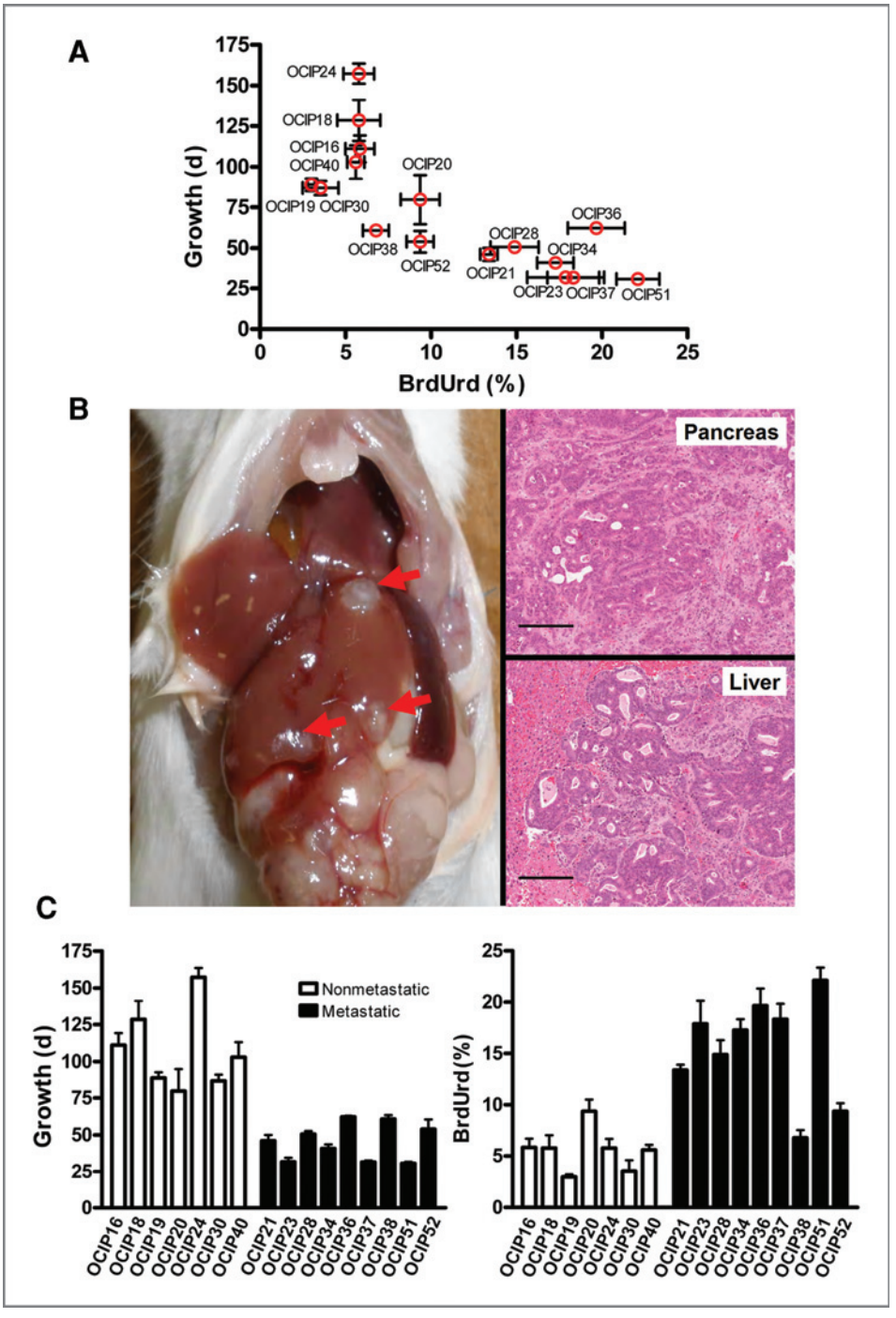

Figure 2. Growth rates correlate with BrdUrd incorporation. A, tumor growth (defined by number of days between orthotopic implantation and growth to ~1-cm diameter) versus BrdUrd incorporation (assessed by immunofluorescence analysis) for 16 models. Each data point represents the mean value of 6 replicate tumors. Error bars, 95% CI. $R^2 = 0.5842$; Pearson, $r = -0.7643$; 95% CI $= -0.9138$ to -0.4324; $P = 0.0006$. B, spontaneous formation of liver metastases (arrows) from OCIP51, grown at the orthotopic site (left). H&E staining of OCIP51 primary tumor (top right) and liver metastasis (bottom right). Scale bars, 200 μm. C, tumor growth (left, $P = 0.0002$) and BrdUrd incorporation (right, $P = 0.0003$) in nonmetastatic and metastatic models. Each data point represents the mean value of 6 replicate tumors. Error bars, 95% CI.

marker cytokeratin 19 (Supplementary Fig. S6). The significance of this finding is not known.

Gene expression profiling of hypoxic versus nonhypoxic models

As shown in Figure 4, there is a strong association between hypoxia, proliferation, and metastasis formation. Because rapid proliferation can cause hypoxia simply by pushing cells away from blood vessels, this might be sufficient to explain the more aggressive behavior of the hypoxic models, as illustrated in Figure 5A (schematic I). Alternatively, hypoxia tolerance might be acquired by some primary xenografts, allowing the accumulation of hypoxic cells that then undergo further reprogramming toward a more invasive or metastatic phenotype (Fig. 5A, schematic II). To explore these alternatives, we selected a panel of genes involved in proliferation, survival, and adaptation to hypoxia that have been previously studied in pancreatic cancers and compared the expression levels in

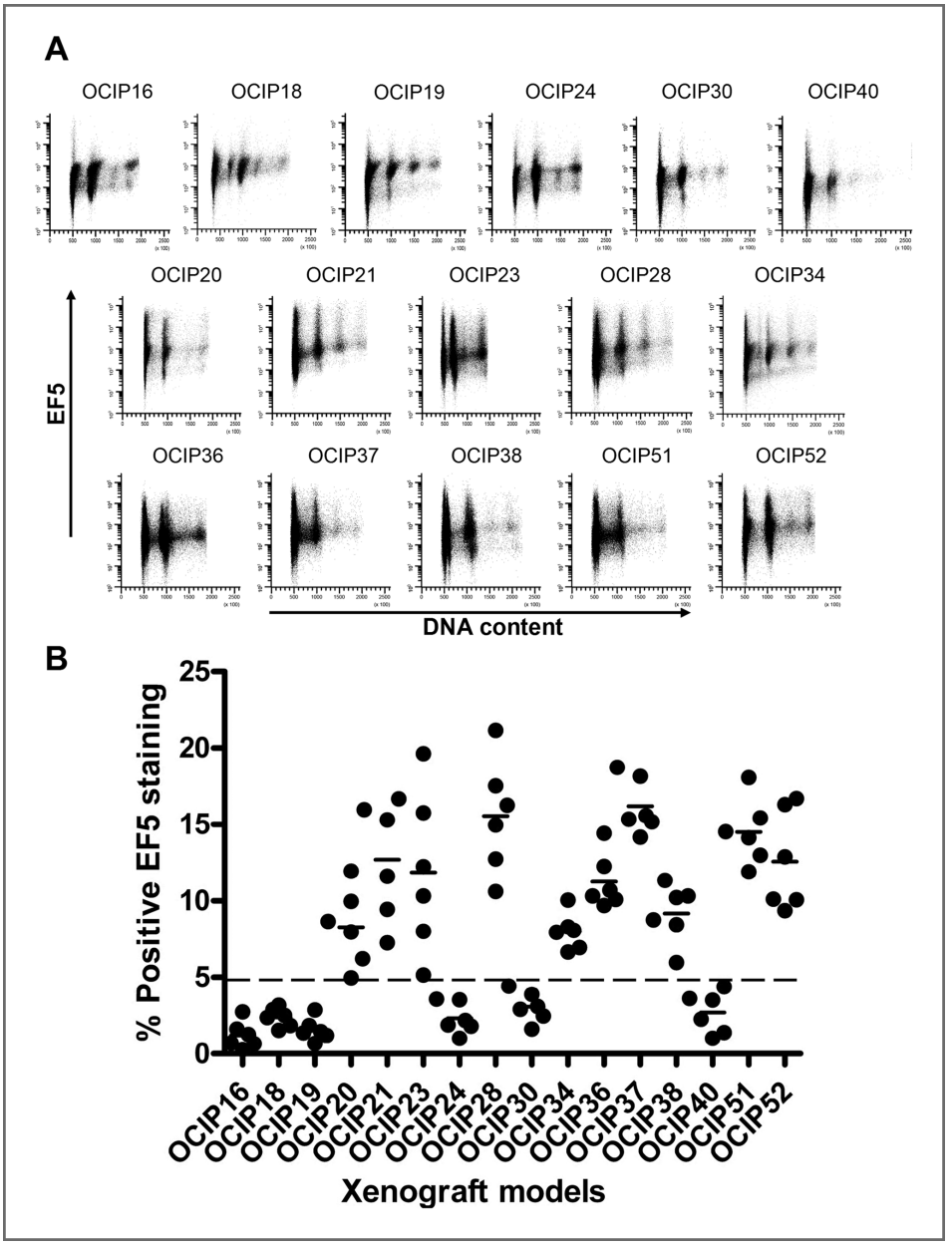

Figure 3. EF5 measurements by flow cytometry. A, representative plots of EF5 labeling versus DNA content for the 16 primary xenografts. Single-cell suspensions of 16 primary xenografts were fixed, stained with 10 μg/mL EF5–Cy5 conjugates and 1 μg/mL DAPI, and analyzed by flow cytometry. EF5 staining was low or absent in OCIP16, 18, 19, 24, 30, and 40 (top), whereas OCIP20, 21, 23, 28, 34, 36, 37, 38, 51, and 52 showed a heterogeneous distribution of positive staining both in the aneuploid cancer cells and in the normal mouse stroma. B, quantification of EF5 staining by flow cytometry in 6 replicate tumors from 16 primary xenografts.

the hypoxic versus nonhypoxic models. As shown in Figure 5B, the hypoxic models showed highly significant increases in the expression of genes coding for proteins involved in cell-cycle regulation (Aurora kinases A and B, cyclin B1; $P < 0.0001$, $P = 0.0012$, $P = 0.0002$, respectively), consistent with their greater BrdUrd incorporation. However, we also found increased expression of genes involved in cell survival (e.g., *Bcl-2*, *XIAP*, and *survivin*), DNA damage repair (*BRCA2* and *Rad51*), and *HIF-1α*, which would favor the acquisition of hypoxia tolerance. Protein–protein interaction analysis also shows strong linkages between hypoxia, proteins involved in cell-cycle regulation, and apoptosis (Fig. 6). Ten of the target proteins have genome maintenance function, and 7 are related to cellular fate and organization. CASP3 directly connects to 6 other target proteins, whereas BCL2 connects to 5. Despite fewer direct connections, SMAD4 and MYC are the most central to the network (as analyzed by all-pairs-shortest-paths in NAViGaTOR). From the target proteins, the highest degree node in the network is MYC (438 interacting partners), HIF1A (296 interacting partners), and TGFBR1 (231 interacting partners).

Discussion

In this article, we identified striking associations between hypoxia and the aggressive features of rapid growth and high metastatic potential in a series of orthotopically grown primary pancreatic cancer xenografts. The highly consistent

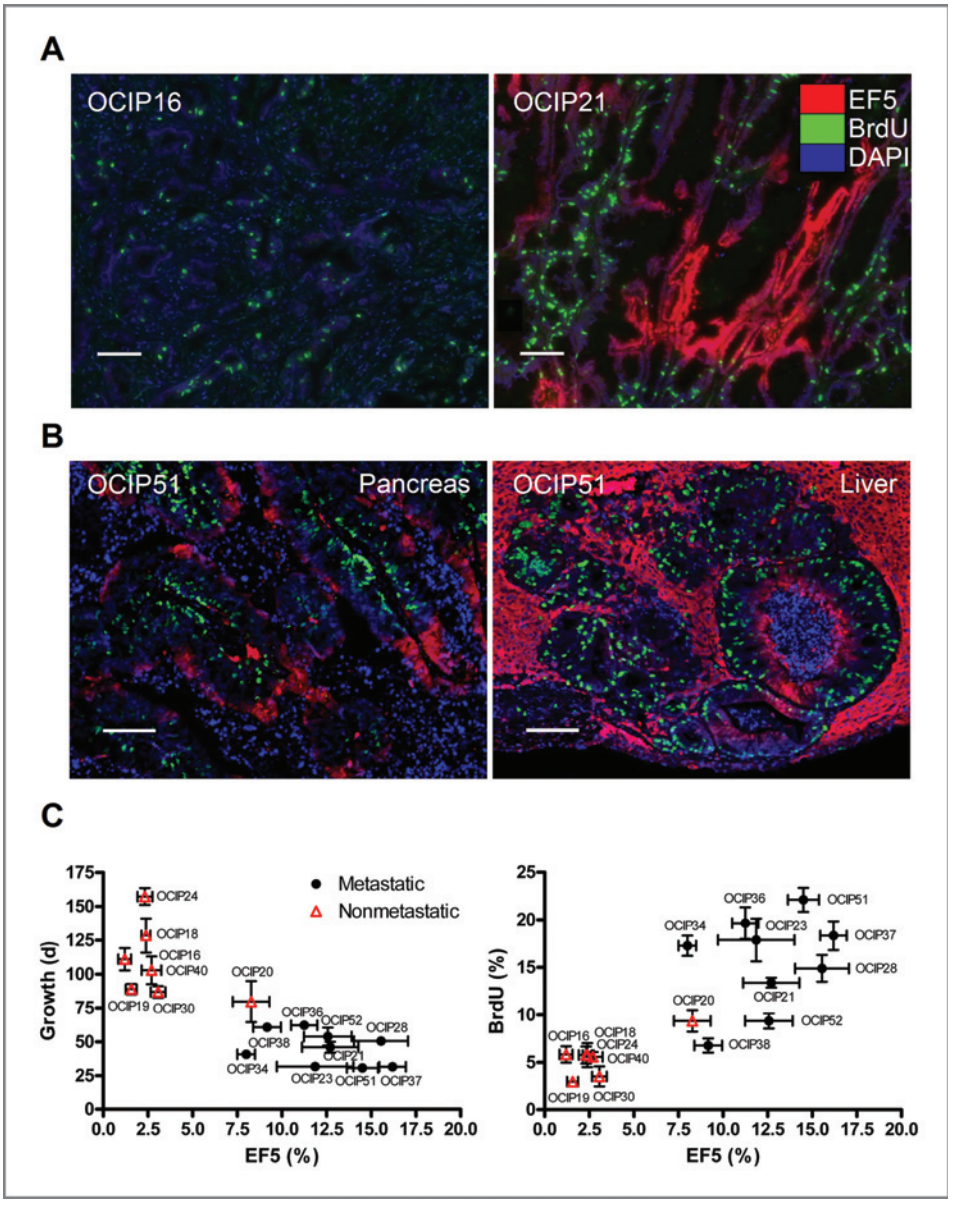

Figure 4. Hypoxia and BrdUrd labeling. A, dual immunofluorescence staining for EF5 and BrdUrd of OCIP16 (left) and OCIP21 (right). Hypoxic regions stained for EF5 (OCIP21) were morphologically similar to the EF5-negative regions, but the BrdUrd labeling was much lower. Scale bars, 100 μm. B, dual immunofluorescence staining for EF5 and BrdUrd of OCIP51 primary tumor (left) and liver metastasis (right). Scale bars, 100 μm. C, tumor growth versus EF5 (left) and BrdUrd labeling versus EF5 (right) for 16 models. Each data point represents the mean value of 6 replicate tumors. Error bars, 95% CI.

results within replicate samples indicate that the underlying mechanisms have a transmissible (genetic or epigenetic) component. This suggests that they reflect, to some extent, biological characteristics of the cancers from which they were derived.

Deficiencies in neovascularization have been linked to the development of hypoxia in some xenograft models, and pancreatic cancers have long been known to show reduced perfusion with radiologic contrast agents (41). However, we did not see a correlation between microvessel density and hypoxia in the primary pancreatic cancer xenografts, suggesting that the failure to develop a vascular system is not directly linked to hypoxia in these tumors.

Within EF5-positive regions, the uptake of BrdUrd was greatly decreased, indicating that hypoxia causes cell-cycle arrest in these tumors. Although there are many previous reports showing this effect in other *in vivo* models (42, 43), we observed a striking increase in the uptake of BrdUrd in the EF5-negative regions of the hypoxic models, relative to the low hypoxia models, that correlated with their more rapid growth and greater metastatic potential. The hypoxic models also showed a highly significant increase in the number of cells expressing cleaved caspase-3, in both EF5-positive and -negative regions, suggesting that the more rapid cell proliferation was, to some extent, counterbalanced by increased cell loss to apoptosis.

Cell survival is compromised under hypoxic conditions. Hypoxia tolerance can occur due to mutation of genes such as *p53* that enhance survival, or through metabolic adaptation in response for example to HIF transcription factors, or the

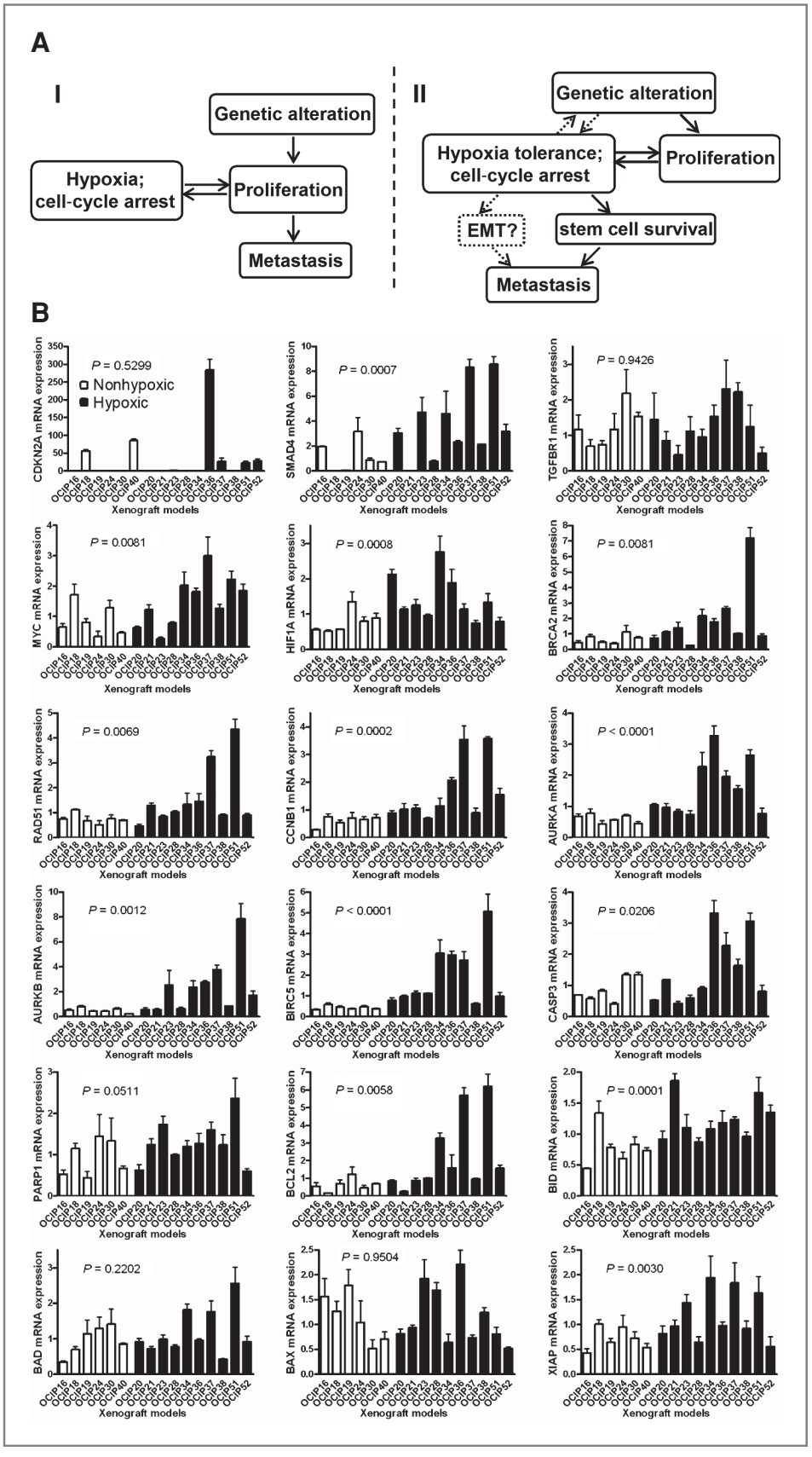

Figure 5. Gene expression profiling of hypoxic versus nonhypoxic models. A, hypothetical mechanisms to explain the correlations between hypoxia, proliferation, and metastasis. B, mRNA expression of genes involved proliferation, survival, and adaptation to hypoxia by qPCR. *P* values of comparison of hypoxic (solid black columns) and nonhypoxic models were shown. Each data point represents the mean value of 3 replicate tumors. Error bars, 95% CI.

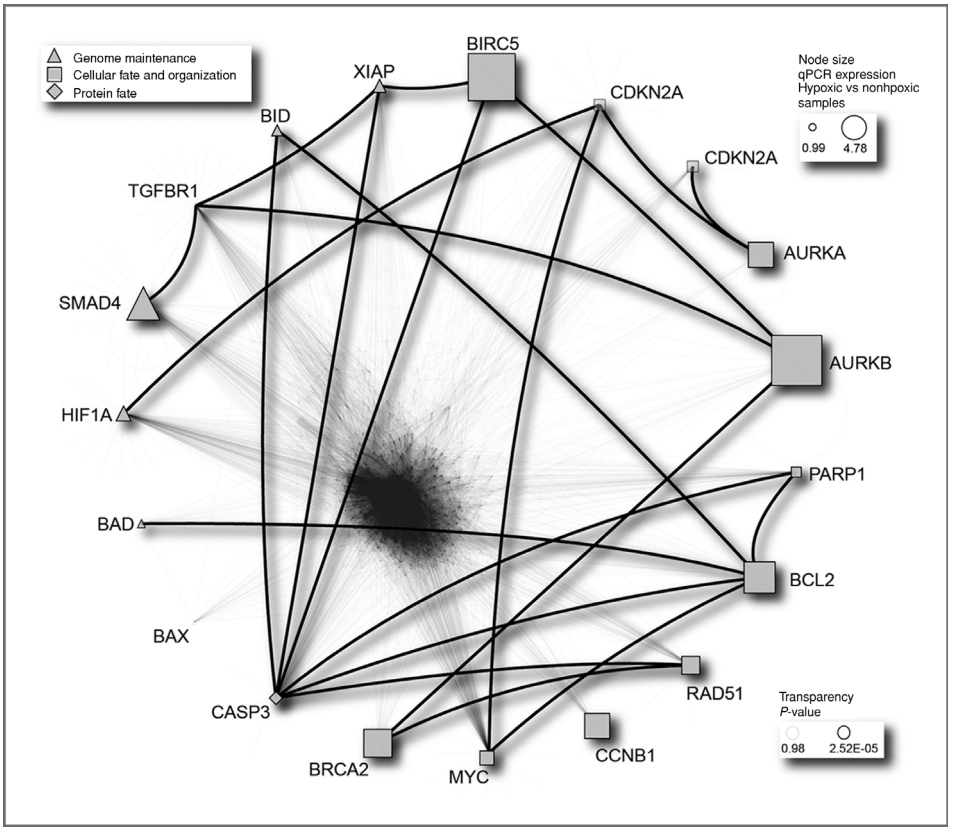

Figure 6. Protein–protein interaction map of qPCR gene validation set. Network comprises 1,562 proteins and 24,389 interactions (partially transparent to reduce complexity), of which 18 target proteins are connected by 28 direct interactions (thick black lines). Note that 2 variants of CDKN2A are listed. Node shape corresponds to GeneOntology biological function as per legend, and 18 target proteins are organized on the circle according to GeneOntology. Node size corresponds to fold difference between hypoxic and nonhypoxic samples on the basis of normalized C_t values, as per legend and methods. Transparency was set to *P* value of the difference, as per legend. All other nodes are viewed as small circles and made transparent to reduce network complexity.

unfolded protein response. Cells adapted to survive hypoxia might then undergo further alterations toward a phenotype with stem cell–like or invasive properties such as EMT that would favor metastasis. Although our results indicate that hypoxia is insufficient to produce EMT in pancreatic cancers, we cannot exclude the possibility that it may play a role under certain conditions.

The association between hypoxia and increased metastatic potential of pancreatic cancer is novel and of major clinical relevance. However, the extent to which hypoxia is driving metastasis, rather than being the consequence of rapid proliferation, remains uncertain. Rapid proliferation pushes cells away from blood vessels so that they become hypoxic and eventually necrotic. Therefore, it is possible that hypoxia is a bystander effect, and that biological aggression seen in the hypoxic models is being driven by proliferation. However, our preliminary analysis, shown in Figure 5, seems to favor the acquisition of hypoxia tolerance because the hypoxic models show increased expression of genes involved in survival and DNA damage response, as well as HIF1A whose transcriptional activation promotes hypoxia tolerance (8). Furthermore, in preliminary experiments, we found that hypoxia persisted during treatment with an MEK (MAP/ERK kinase) inhibitor that potently inhibits cell-cycle progression (29), suggesting that some degree of hypoxia tolerance exists in these models (Supplementary Fig. S7).

Detailed investigation of the possible genetic mechanisms linking hypoxia to aggressive growth is ongoing, including DNA sequencing as part of the International Cancer Genome Consortium Pancreatic Cancer Genome Project (44).

Clinical implications

Our results predict that the presence of hypoxia in patients undergoing surgical resection for pancreatic cancer carries a high risk of recurrence. Although the follow-up data are limited, we observed a trend for longer survival in the patient donors of the low hypoxia tumors (Supplementary Fig. S8). However, TNM stages for patients enrolled in this study are higher than those that are typical for patients undergoing pancreatectomy (45), probably because insufficient xenograft material was available from early-stage tumors, which may account for the relatively poor survival. To determine the prognostic significance of hypoxia in pancreatic cancer patients, we have started a clinical trial that administers the nitroimidazole probe pimonidazole to patients undergoing pancreatectomy (46, 47). Because primary xenografts are being established from these patients, this study will also allow us to determine the extent to which hypoxia in the patient samples is correlated with hypoxia measurements made in the corresponding primary xenografts.

Regardless of whether hypoxia plays a significant role driving metastasis, or is simply the consequence of rapid growth, BrdUrd-negative cells in hypoxic regions are expected to be resistant to gemcitabine, the mainstay of adjuvant chemotherapy protocols, because this drug is incorporated during S-phase. Significantly, cell-cycle arrest in relation to

hypoxia occurs in early liver metastases from orthotopic primary pancreatic cancer xenografts (Fig. 4B). If these noncycling cells can reenter the cell cycle following the destruction of proliferating, better oxygenated cells, then the tumor would be expected to repopulate. The overall effect of adjuvant treatment might therefore be to delay cancer recurrence, rather than eliminate all residual cancer cells, and results from randomized clinical trials suggest that this might indeed be the case (48). If so, a logical strategy would be to combine classic chemotherapy drugs such as gemcitabine with bioreductive agents that show selective toxicity toward hypoxic cells (49, 50).

In conclusion, results shown in this article point toward important mechanisms that link the development of hypoxia to biological aggression in pancreatic cancer patients. Elucidation of the underlying mechanisms is likely to suggest novel therapeutic interventions to improve patient outcome. However, if the results seen in the orthotopic primary xenografts are confirmed in pancreatectomy patients, then they predict that improved patient outcome might be achieved by incorporating hypoxia-targeted agents into existing adjuvant or neoadjuvant treatment protocols, regardless of the underlying molecular mechanisms.

Disclosure of Potential Conflicts of Interest

No potential conflicts of interest were disclosed.

Acknowledgments

The authors thank Drs. Richard P. Hill, Steven Gallinger, and Ming Tsao for many helpful discussions. The authors also thank Pinjiang Cao, Lucy Zhang, Jing Xu, Ni Liu, and Emin Ibrahimov for their excellent technical assistance.

Grant Support

This work was supported by John and Esther Loewen Family Fund and a research grant from the Ontario Institute for Cancer Research. Computational analyses and infrastructure were supported in part by Ontario Research Fund GL2, Canada Foundation for Innovation, Canada Research Chair program, and IBM. This research was funded in part by the Ontario Ministry of Health and Long Term Care. The views expressed do not necessarily reflect those of the Ontario Ministry of Health and Long Term Care.

The costs of publication of this article were defrayed in part by the payment of page charges. This article must therefore be hereby marked *advertisement* in accordance with 18 U.S.C. Section 1734 solely to indicate this fact.

Received November 8, 2010; revised January 6, 2011; accepted February 7, 2011; published OnlineFirst February 22, 2011.

References

1. Vaupel P, Mayer A. Hypoxia in cancer: significance and impact on clinical outcome. Cancer Metastasis Rev 2007;26:225–39.
2. Brizel DM, Sibley GS, Prosnitz LR, Scher RL, Dewhirst MW. Tumor hypoxia adversely affects the prognosis of carcinoma of the head and neck. Int J Radiat Oncol Biol Phys 1997;38:285–9.
3. Brown JM. Tumor microenvironment and the response to anticancer therapy. Cancer Biol Ther 2002;1:453–8.
4. Fyles A, Milosevic M, Hedley D, Pintilie M, Levin W, Manchul L, et al. Tumor hypoxia has independent predictor impact only in patients with node-negative cervix cancer. J Clin Oncol 2002;20:680–7.
5. Hockel M, Schlenger K, Aral B, Mitze M, Schaffer U, Vaupel P. Association between tumor hypoxia and malignant progression in advanced cancer of the uterine cervix. Cancer Res 1996;56:4509–15.
6. Brizel DM, Scully SP, Harrelson JM, Layfield LJ, Bean JM, Prosnitz LR, et al. Tumor oxygenation predicts for the likelihood of distant metastases in human soft tissue sarcoma. Cancer Res 1996;56:941–3.
7. Graeber TG, Osmanian C, Jacks T, Housman DE, Koch CJ, Lowe SW, et al. Hypoxia-mediated selection of cells with diminished apoptotic potential in solid tumours. Nature 1996;379:88–91.
8. Harris AL. Hypoxia—a key regulatory factor in tumour growth. Nat Rev Cancer 2002;2:38–47.
9. Wouters BG, Koritzinsky M. Hypoxia signalling through mTOR and the unfolded protein response in cancer. Nat Rev Cancer 2008;8:851–64.
10. Yachida S, Jones S, Bozic I, Antal T, Leary R, Fu B, et al. Distant metastasis occurs late during the genetic evolution of pancreatic cancer. Nature 2010;467:1114–7.
11. Lunt SJ, Chaudary N, Hill RP. The tumor microenvironment and metastatic disease. Clin Exp Metastasis 2009;26:19–34.
12. Yang MH, Wu MZ, Chiou SH, Chen PM, Chang SY, Liu CJ, et al. Direct regulation of TWIST by HIF-1alpha promotes metastasis. Nat Cell Biol 2008;10:295–305.
13. Sullivan R, Graham CH. Hypoxia-driven selection of the metastatic phenotype. Cancer Metastasis Rev 2007;26:319–31.
14. Lester RD, Jo M, Montel V, Takimoto S, Gonias SL. uPAR induces epithelial-mesenchymal transition in hypoxic breast cancer cells. J Cell Biol 2007;178:425–36.
15. Sahlgren C, Gustafsson MV, Jin S, Poellinger L, Lendahl U. Notch signaling mediates hypoxia-induced tumor cell migration and invasion. Proc Natl Acad Sci U S A 2008;105:6392–7.
16. Klymkowsky MW, Savagner P. Epithelial-mesenchymal transition: a cancer researcher's conceptual friend and foe. Am J Pathol 2009;174:1588–93.
17. Cannito S, Novo E, Compagnone A, Valfrè di Bonzo L, Busletta C, Zamara E, et al. Redox mechanisms switch on hypoxia-dependent epithelial-mesenchymal transition in cancer cells. Carcinogenesis 2008;29:2267–78.
18. Hermann PC, Huber SL, Herrler T, Aicher A, Ellwart JW, Guba M, et al. Distinct populations of cancer stem cells determine tumor growth and metastatic activity in human pancreatic cancer. Cell Stem Cell 2007;1:313–23.
19. Rasheed ZA, Yang J, Wang Q, Kowalski J, Freed I, Murter C, et al. Prognostic significance of tumorigenic cells with mesenchymal features in pancreatic adenocarcinoma. J Natl Cancer Inst 2010;102:340–51.
20. Heddleston JM, Li Z, McLendon RE, Hjelmeland AB, Rich JN. The hypoxic microenvironment maintains glioblastoma stem cells and promotes reprogramming towards a cancer stem cell phenotype. Cell Cycle 2009;8:3274–84.
21. Matsumoto K, Arao T, Tanaka K, Kaneda H, Kudo K, Fujita Y, et al. mTOR signal and hypoxia-inducible factor-1 alpha regulate CD133 expression in cancer cells. Cancer Res 2009;69:7160–4.
22. Hill RP, Marie-Egyptienne DT, Hedley DW. Cancer stem cells, hypoxia and metastasis. Semin Radiat Oncol 2009;19:106–11.
23. Hiraoka N, Ino Y, Sekine S, Tsuda H, Shimada K, Kosuge T, et al. Tumour necrosis is a postoperative prognostic marker for pancreatic cancer patients with a high interobserver reproducibility in histological evaluation. Br J Cancer 2010;103:1057–65.
24. Iakovlev VV, Pintilie M, Morrison A, Fyles AW, Hill RP, Hedley DW. Effect of distributional heterogeneity on the analysis of tumor hypoxia based on carbonic anhydrase IX. Lab Invest 2007;87:1206–17.
25. Koong AC, Mehta VK, Le QT, Fisher GA, Terris DJ, Brown JM, et al. Pancreatic tumors show high levels of hypoxia. Int J Radiat Oncol Biol Phys 2000;48:919–22.
26. Ng SS, Tsao MS, Nicklee T, Hedley DW. Wortmannin inhibits pkb/akt phosphorylation and promotes gemcitabine antitumor activity in

orthotopic human pancreatic cancer xenografts in immunodeficient mice. Clin Cancer Res 2001;7:3269–75.
27. Yau CY, Wheeler JJ, Sutton KL, Hedley DW. Inhibition of integrin-linked kinase by a selective small molecule inhibitor, QLT0254, inhibits the PI3K/PKB/mTOR, Stat3, and FKHR pathways and tumor growth, and enhances gemcitabine-induced apoptosis in human orthotopic primary pancreatic cancer xenografts. Cancer Res 2005;65: 1497–504.
28. Cao P, Maira SM, Garcia-Echeverria C, Hedley DW. Activity of a novel, dual PI3-kinase/mTor inhibitor NVP-BEZ235 against primary human pancreatic cancers grown as orthotopic xenografts. Br J Cancer 2009;100:1267–76.
29. Chang Q, Chapman MS, Miner JN, Hedley DW. Antitumour activity of a potent MEK inhibitor RDEA119/BAY 869766 combined with rapamycin in human orthotopic primary pancreatic cancer xenografts. BMC Cancer 2010;10:515.
30. Koch CJ. Measurement of absolute oxygen levels in cells and tissues using oxygen sensors and 2-nitroimidazole EF5. Methods Enzymol 2002;352:3–31.
31. Vukovic V, Haugland HK, Nicklee T, Morrison AJ, Hedley DW. Hypoxia-inducible factor-1alpha is an intrinsic marker for hypoxia in cervical cancer xenografts. Cancer Res 2001;61:7394–8.
32. Allalunis-Turner MJ, Siemann DW. Recovery of cell subpopulations from human tumour xenografts following dissociation with different enzymes. Br J Cancer 1986;54:615–22.
33. Koch CJ. Importance of antibody concentration in the assessment of cellular hypoxia by flow cytometry: EF5 and pimonidazole. Radiat Res 2008;169:677–88.
34. Pham NA, Magalhaes JM, Do T, Schwock J, Dhani N, Cao PJ, et al. Activation of Src and Src-associated signaling pathways in relation to hypoxia in human cancer xenograft models. Int J Cancer 2009;124: 280–6.
35. Vandesompele J, De Preter K, Pattyn F, Poppe B, Van Roy N, De Paepe A, et al. Accurate normalization of real-time quantitative RT-PCR data by geometric averaging of multiple internal control genes. Genome Biol 2002;3:RESEARCH0034.
36. Brown KR, Jurisica I. Unequal evolutionary conservation of human protein interactions in interologous networks. Genome Biol 2007; 8:R95.
37. Brown KR, Otasek D, Ali M, McGuffin MJ, Xie W, Devani B, et al. NAViGaTOR: Network Analysis, Visualization and Graphing Toronto. Bioinformatics 2009;25:3327–9.
38. Kavanagh MC, Tsang V, Chow S, Koch C, Hedley D, Minkin S, et al. A comparison in individual murine tumors of techniques for measuring oxygen levels. Int J Radiat Oncol Biol Phys 1999;44: 1137–46.
39. Chang Q, Chen E, Hedley DW. Effects of combined inhibition of MEK and mTOR on downstream signaling and tumor growth in pancreatic cancer xenograft models. Cancer Biol Ther 2009;8:1893–901.
40. Harikumar KB, Kunnumakkara AB, Sethi G, Diagaradjane P, Anand P, Pandey MK, et al. Resveratrol, a multitargeted agent, can enhance antitumor activity of gemcitabine *in vitro* and in orthotopic mouse model of human pancreatic cancer. Int J Cancer 127;257–68.
41. Gortenuti G, Cavallini G, Vantini I, Angelini G, Piubello W, Frasson F, et al. Angiography in chronic pancreatitis and pancreatic cancer. A critical evaluation. Am J Gastroenterol 1978;70:620–6.
42. Carmeliet P, Dor Y, Herbert JM, Fukumura D, Brusselmans K, Dewerchin M, et al. Role of HIF-1alpha in hypoxia-mediated apoptosis, cell proliferation and tumour angiogenesis. Nature 1998; 394:485–90.
43. Evans SM, Hahn SM, Magarelli DP, Koch CJ. Hypoxic heterogeneity in human tumors: EF5 binding, vasculature, necrosis, and proliferation. Am J Clin Oncol 2001;24:467–72.
44. Hudson TJ, Anderson W, Artez A, Barker AD, Bell C, Bernabé RR, et al. International network of cancer genome projects. Nature 2010; 464:993–8.
45. Cleary SP, Gryfe R, Guindi M, Greig P, Smith L, Mackenzie R, et al. Prognostic factors in resected pancreatic adenocarcinoma: analysis of actual 5-year survivors. J Am Coll Surg 2004;198: 722–31.
46. Azuma Y, Chou SC, Lininger RA, Murphy BJ, Varia MA, Raleigh JA. Hypoxia and differentiation in squamous cell carcinomas of the uterine cervix: pimonidazole and involucrin. Clin Cancer Res 2003;9:4944–52.
47. Nordsmark M, Loncaster J, Aquino-Parsons C, Chou SC, Gebski V, West C, et al. The prognostic value of pimonidazole and tumour pO_2 in human cervix carcinomas after radiation therapy: a prospective international multi-center study. Radiother Oncol 2006;80:123–31.
48. Oettle H, Post S, Neuhaus P, Gellert K, Langrehr J, Ridwelski K, et al. Adjuvant chemotherapy with gemcitabine vs observation in patients undergoing curative-intent resection of pancreatic cancer: a randomized controlled trial. JAMA 2007;297:267–77.
49. Tredan O, Garbens AB, Lalani AS, Tannock IF. The hypoxia-activated ProDrug AQ4N penetrates deeply in tumor tissues and complements the limited distribution of mitoxantrone. Cancer Res 2009;69:940–7.
50. Marcu L, Olver I. Tirapazamine: from bench to clinical trials. Curr Clin Pharmacol 2006;1:71–9.